
Article:
Dixon Wilkins, M.C. orcid.org/0000-0003-1520-7672, Stennett, M.C., McCloy, J.S. et al. (1 more author) (2023) Solid solubility in the CeTi2O6–CeTiNbO6 system: a multi-element X-ray spectroscopic study. MRS Advances, 8 (7). pp. 267-273. ISSN 2731-5894

https://doi.org/10.1557/s43580-023-00532-2

MRS Advances
https://doi.org/10.1557/s43580-023-00532-2

ORIGINAL PAPER

Solid solubility in the $CeTi_2O_6$–$CeTiNbO_6$ system: A multi-element X-ray spectroscopic study

M. C. Dixon Wilkins[1,2] · M. C. Stennett[1] · J. S. McCloy[2] · C. L. Corkhill[1]

Received: 23 January 2023 / Accepted: 21 February 2023

Abstract

In order to investigate the limits of solid solubility between Ce-brannerite ($CeTi_2O_6$) and Ce-aeschynite ($CeTiNbO_6$), materials in the system $CeTi_{2-x}Nb_xO_6$ have been produced by a solid state route and characterised by XRD and XANES at the Ce L_3-, Ti K- and Nb K-edges, including Rietveld method refinements and linear combination fitting. Significant solid solubility was observed at the brannerite end, with near-single-phase brannerite observed for $x = 0.2$, 0.4, and only minor aeschynite observed where $x = 0.6$ which was identified as exceeding the limit of solubility of Nb. All Nb was present as Nb^{5+}, with the substitution of Nb^{5+} into the brannerite structure permitted by the reduction of the same fraction of Ce^{4+} to Ce^{3+}. This work expands the crystal chemistry of the titanate brannerites, with Ce-site oxidation states of less than 4+ being possible where sufficient charge-balancing species are available on the Ti-site.

Introduction

Research examining materials for long-term immobilisation of radionuclides from highly active nuclear wastes is ongoing, particularly with respect to matrices for immobilisation of the actinide species including both Pu and the minor actinides, *e.g.* those that will contribute significantly to the long-term radiotoxicity of spent fuel. A significant body of work exists examining candidate host materials for $Pu^{3+/4+}$ with current favored ceramic materials including zirconolite [1–3], pyrochlore [4–6], and brannerite [7–9] ceramics, as either single-phase ceramics or part of a multiphase waste-form. Materials for immobilisation of the minor actinides (chiefly Am^{3+}, Cm^{3+}, and $Np^{4+/5+}$) have received relatively less attention, though are likely compatible with many of the same materials, particularly pyrochlores [5, 10, 11] and zirconolites [11, 12]. Due to the highly radioactive nature of Pu and the minor actinides, chemical surrogates (*e.g.* $Ce^{3+/4+}$ for $Pu^{3+/4+}$, REE^{3+} for trivalent actinides) for these elements are utilised in preliminary works, with Ce most commonly used as a surrogate for Pu on account of their similar chemistry and available oxidation states in oxide systems.

A range of synthetic Ce-, U- and Th-brannerites (ATi_2O_6) have been previously examined, including A^{4+}, mixed $A^{3+/5+}$ and A^{5+} with Ti-site charge balancing. However, little work has examined the possibility of A^{3+} only brannerites, with charge neutrality ensured by higher valence substitutions on the Ti-site. If the brannerite structure is flexible with respect to an average A-site oxidation state of less than 4+, it would be of particular interest for the immobilisation of mixed valence Pu and/or mixed minor actinide waste streams. Previous work examining the limits of ion size in Th-brannerite reported solubility of 0.25 f.u. (formula units) Nb^{5+} and Al^{3+} when substituting for 0.5 f.u. of Ti^{4+}, corresponding to a slight decrease in average Ti-site ionic radius, and solubility of approximately 0.2 f.u. of Sn^{+4} for Ti^{4+}, a slight increase of the average Ti-site ionic radius [13].

Aeschynite structures ($ATi(Nb,Ta)O_6$, where A = trivalent rare earth elements, REE^{3+}) form for the larger REE, with the euxenite structure (also $REE^{3+}Ti(Nb,Ta)O_6$) being favored for the smaller REE [14], with the transition between the two structures occurring between Dy and Ho. Given the similarities in ionic radius and dominance of the trivalent state in both the lanthanides and minor actinides, it is likely significant actinide solubility will occur in appropriate $ATi(Nb,Ta)O_6$ materials, making them candidate materials for immobilisation of high actinide content wastes [15].

✉ C. L. Corkhill
c.corkhill@sheffield.ac.uk

1 Immobilisation Science Laboratory, Department of Materials Science and Engineering, University of Sheffield, Sheffield, UK

2 School of Mechanical and Materials Engineering, Washington State University, PO Box 642920, Pullman, WA 99164, USA

Published online: 08 March 2023

The complexity of Ce redox chemistry in these and similar systems is well established. Even when starting from a Ce^{4+} precursor (*e.g.* CeO_2), a significant fraction of Ce^{3+} can form at the synthesis temperature, with some fraction able to be quenched into the brannerite structure [16], even at relatively slow cooling rates of 5 or 10 °C min^{-1} [17, 18], with charge neutrality ensured by O vacancies. As brannerites containing U^{5+} can be stabilised by inclusion of lower valence charge compensating dopants (*e.g.* the $U_{0.5}REE_{0.5}Ti_2O_6$ and $UTi_{2-x}Al_xO_6$ systems [9, 19, 20]), the aim of the current study was to determine whether Ce-brannerites with mean Ce oxidation states significantly below 4+ could be stabilised by doping with a higher valent cation. Moreover, this study examined the possibility of Ce-aeschynites with mean Ce oxidation states significantly above 3+, stabilised by an excess of Ti^{4+} on the Ti/Nb site.

Materials and methods

Materials were produced following a cold-press and sinter solid state route. Stoichiometric amounts of oxides (CeO_2, Nb_2O_5 and TiO_2) were weighed according to the target compositions ($CeTi_{2-x}Nb_xO_6$, $x = 0$–1, $\Delta x = 0.2$) and homogenised by planetary milling (Fritsch Pulverisette 7), utilising ZrO_2 mill pots and media, and isopropanol as a carrier fluid, for 10 min at 500 rpm. Approximately 0.5 g of the dried milled material of each composition was then pressed into 10 mm diameter pellets under 2 tonnes of weight. Pellets were heat treated in air at 1350 °C for two heat treatments of 24 h (heating and cooling at 5 °C min^{-1}), with the pellets being broken up, reground and again pressed into pellets after the first heat treatment.

Powder XRD patterns were collected with a Bruker D2 Phaser diffractometer, utilising Ni-filtered Cu K_α radiation. Rietveld method refinements were utilised to examine crystal chemical changes induced on inclusion of Nb into the brannerite structure. Ce L_3-edge, Ti K-edge and Nb K-edge spectra were collected at NSLS-II beamline 6-BM (Brookhaven National Laboratory, USA). Transmission mode measurements were performed at room temperature on pellets comprising sufficient material to form one absorption length and polyethylene glycol (PEG), as an inert, low-absorbing binder. Data were normalised and analysed in Athena, part of the Demeter software suite [21], and XAS Viewer, part of the Larch software suite [22].

Results

X-ray diffraction

Based on analysis of their diffraction patterns (see Fig. 1), in materials targeting $0 \leq x \leq 0.4$, *i.e.* $CeTi_2O_6$, $CeTi_{1.8}Nb_{0.2}O_6$

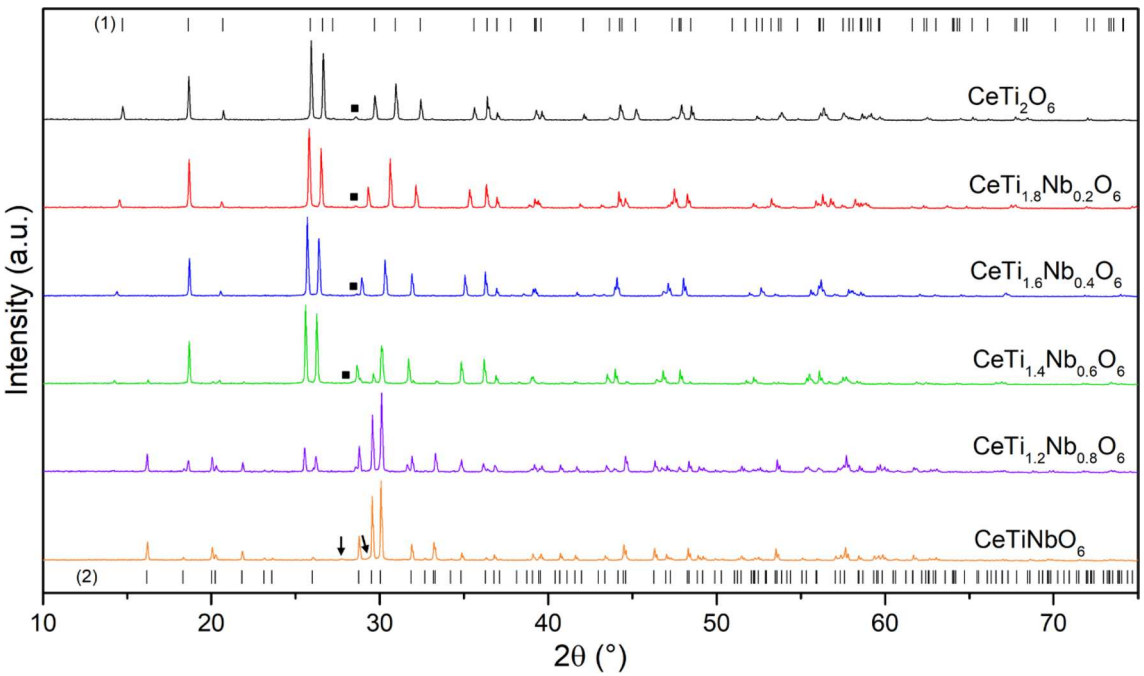

Fig. 1 XRD patterns of materials batched following the solid solution $CeTi_{2-x}Nb_xO_6$. The positions of the reflections of $CeTi_2O_6$ (1) are marked above, those of $CeTiNbO_6$ (2) below. The positions of the diagnostic reflection of CeO_2 are marked with black squares, those of $CeNbO_4$ with arrows

and $CeTi_{1.6}Nb_{0.4}O_6$, near-single-phase brannerite was formed, with a small fraction of CeO_2 also observed (0.6(1), 0.3(1) and 0.4(1) wt% CeO_2, respectively). An increase in the brannerite unit cell parameters was apparent, with shifts to lower 2θ observed for many reflections. This observation gave an initial indication of the solubility of Nb in Ce-brannerite. When the targeted Nb content was increased to $x=0.6$ ($CeTi_{1.4}Nb_{0.6}O_6$), brannerite remained the majority phase, alongside small fractions of aeschynite and CeO_2 (7.2(2) and 1.8(2) wt%, respectively). Further attempted substitution of Nb led to increased fractions of aeschynite, with the material targeting $x=0.8$ comprising 65.6(6) wt% aeschynite and 34.4(6) wt% brannerite only, suggesting that this composition exceeds the limit of solubility of Nb in Ce-brannerite. The material targeting the end-member aeschynite $CeTiNbO_6$ contained aeschynite as the major phase, with $CeNbO_4$ observed as a minor phase (1.5(2) wt%).

On consideration of the phases produced, it was apparent that Nb had significant solubility in Ce-brannerite, with the limit of solubility likely around 0.6 f.u., given the observation of a small fraction of aeschynite in the material targeting $CeTi_{1.4}Nb_{0.6}O_6$. This is in good agreement with the as-refined unit cell parameters (see S.I. Table 1 and S.I. Fig. 2), where linear increases in the unit cell volume and *b* and *c* parameters and a linear decrease in the cell angle β (relating to an increase in overall unit cell volume) were observed as the targeted Nb loading was increased from 0 f.u. to 0.6 f.u., corresponding to increases in average Ce-site and Ti-site ionic radii (6 coordinate ionic radii: Ce^{4+}, 0.87 Å; Ce^{3+}, 1.01 Å; Ti^{+4}, 0.605 Å; Nb^{+5}, 0.64 Å [23]). The *a* parameter also increased on increasing substitution of Nb, but the overall change was of a much smaller magnitude. The trends observed in the unit cell parameters also suggest the limit of solubility is just below 0.6 f.u. Nb, with the *b*, *c* and β parameters and overall unit cell volume of the brannerite phase remaining approximately the same between 0.6 and 0.8 f.u. targeted Nb loading. The as-refined phase fractions in each material are detailed in S.I. Table 1 and S.I. Fig. 1.

Elemental speciation

Nb K-edge XANES

Though Nb^{5+} predominates in oxide systems when heated in air, it was thought that some reduction of Nb^{5+} by the re-oxidation of Ce^{3+} to Ce^{4+} on cooling may have been possible. Nb K-edge XANES was utilised to examine the Nb oxidation states in the produced materials. Examination of the collected spectra and comparison to reference compounds of known Nb oxidation state (Nb metal, $Nb^{2+}O$, $Nb^{4+}O_2$, and $Nb^{5+}{}_2O_5$) suggested that Nb^{5+} was the dominant oxidation state in the materials produced here, given the position of the absorption edges and presence of the pre-edge shoulder indicative of Nb^{5+} (see Fig. 2).

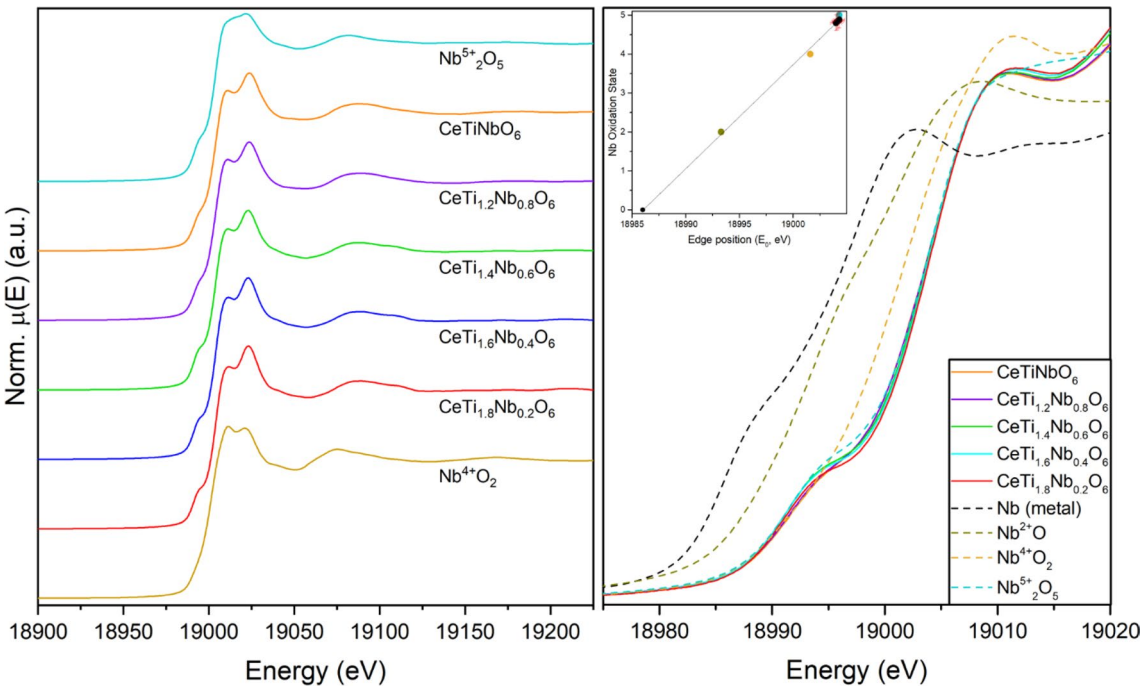

Fig. 2 Left: Nb K-edge XANES spectra of materials in the $CeTi_{2-x}Nb_xO_6$ system, alongside the spectra of $Nb^{5+}{}_2O_5$ and $Nb^{4+}O_2$ reference compounds. Right: detailed view of the absorption edge, with linear regression of edge position against oxidation state inset (utilising Nb metal, $Nb^{2+}O$, $Nb^{4+}O_2$, and $Nb^{5+}{}_2O_5$ as reference compounds)

As the position of the Nb K-edge is strongly correlated with the Nb oxidation state, a linear regression was performed comparing the position of the absorption edges (E_0, defined as the position of the maximum of the first derivative of the spectra) to those of the reference compounds of known Nb oxidation state (see Fig. 2, inset). The mean Nb oxidation state of all materials produced here was determined to be, within error, 5+.

Ti K-edge XANES

Given the expansion of the brannerite unit cell on inclusion of Nb compared to the undoped Ce-brannerite, it was anticipated that some relaxation of the distortion of $(Ti,Nb)O_6$ octahedra may have occurred. The Ti K absorption edge is characterised by the appearance of one or more pre-edge features approximately 15 ± 3 eV before the main edge. These pre-edge features are often attributed to transitions from the Ti 1 *s* orbitals to either Ti 3*d* or O 2*p* orbitals, though are better understood in the context of a more complex band structure [24, 25]. In both interpretations, the symmetry (or lack thereof) around Ti centres is key to the intensity and shape of the pre-edge, with non-centrosymmetric coordination of Ti (*e.g.* tetrahedral environments) leading to higher intensity features than highly centrosymmetric environments (*e.g.* regular octahedra).

The pre-edge features identified in the Ti K-edge spectra of these materials were of relatively low intensity and comprised multiple distinct peaks, indicative of octahedral coordination of Ti in all materials (see Fig. 3), as expected from their crystal structures. The pre-edge features observed in compositions where brannerite predominated, with $0 \leq x \leq 0.6$, had obvious differences to those of aeschynite-rich compositions, where $x = 0.8$, 1.0. The origins of pre-edge features characteristic of Ti in distorted octahedral environments are complex and dependent on the type and degree of polyhedral distortions [24], however, qualitative interpretations can still be made.

When comparing the pre-edge features for the brannerite-rich materials (up to $CeTi_{1.4}Nb_{0.6}O_6$), decreases in intensity of the pre-edge features are observed, along with a change in shape for the most intense feature at approximately 4970 eV. This likely relates to a partial relaxation of the $(Ti,Nb)O_6$ octahedra, facilitated by the lattice expansion observed on increased incorporation of Nb^{5+} and reduction to Ce^{3+}. As expected from the phase assemblage, the spectrum of the material targeting $CeTi_{1.2}Nb_{0.8}O_6$ (65.6(6) wt% aeschynite, 34.4(6) wt% brannerite) displayed features approximately intermediate between the brannerite-structured materials and the $CeTiNbO_6$ end-member.

The lower relative pre-edge feature intensities observed for the aeschynite-dominant materials is a result of the less distorted nature of the $(Ti,Nb)O_6$ features in the $CeTiNbO_6$

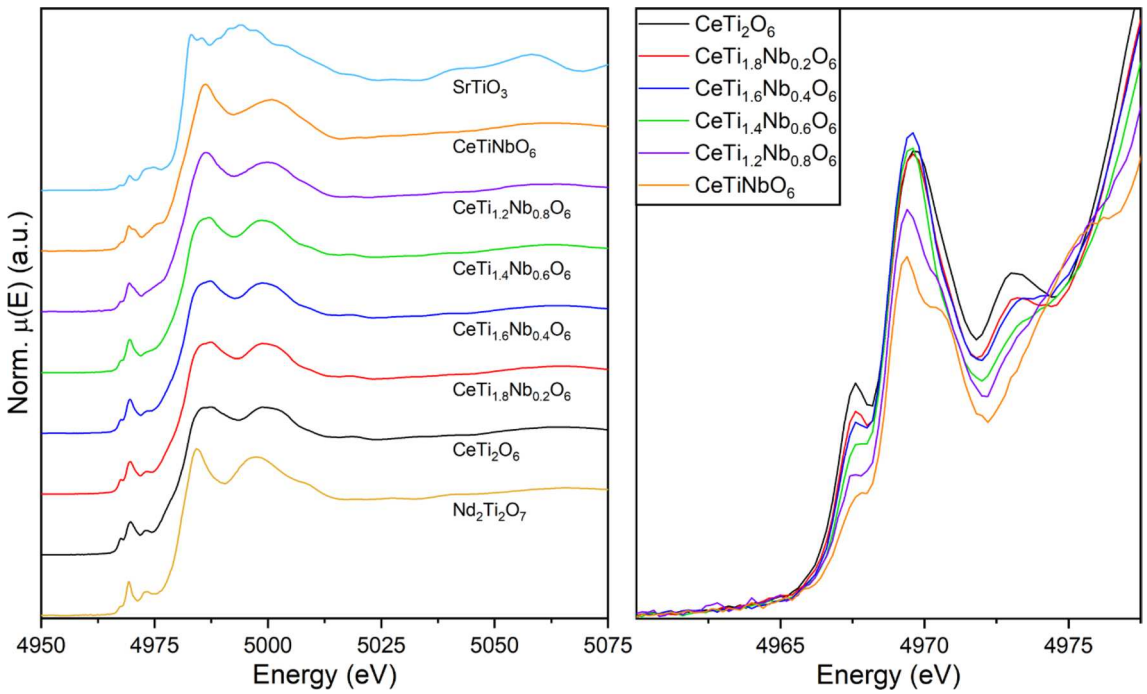

Fig. 3 Left: Ti K-edge XANES spectra of materials in the system $CeTi_{2-x}Nb_xO_6$, alongside the spectra of $SrTiO_3$ and $Nd_2Ti_2O_7$ reference compounds, containing Ti^{4+} in octahedral coordination environments only. Right: detailed view of the pre-edge features observed in the spectra of the materials produced here

structure, relative to those in Ce-brannerite. For example, in $CeTiNbO_6$ the quadratic elongation of the $(Ti,Nb)O_6$ octahedra is 1.0246, the bond angle variance 75.887° [2]; compared to 1.0362 and 115.156° [2] for Ce-brannerite (ICSD entries #20600 and #1702279, respectively).

Ce L_3-edge XANES

The oxidation state of Ce in the phases produced is of importance when discussing their relevance to immobilisation of minor actinides and/or mixed valence Pu. Given the solubility of Nb^{5+} in the brannerite structure, it was anticipated that a significant fraction of Ce^{3+} would be present.

On initial examination of the Ce L_3-edge spectra (see Fig. 4), it was apparent that increasing substitution of Nb^{5+} into the brannerite structure had led to significant reduction of Ce^{4+}, with increased intensity observed in feature C (intense in Ce^{3+} compounds, weak or very weak in Ce^{4+} compounds), and decreases in the relative intensities of features A and B (strong in Ce^{4+} compounds, weak or not present in Ce^{3+} compounds). Linear combination fitting (LCF) utilising a range of reference compounds of known Ce oxidation state ($Ce^{4+}O_2$, $SrCe^{4+}O_3$, $Ce^{3+}PO_4$, $Ce^{3+}{}_2Ti_2O_7$ and $Ce^{3+}{}_2Si_2O_7$, see S.I. Table 2) was performed to quantify the observed changes in overall Ce oxidation state on incorporation of Nb.

It should be noted that some materials examined here did contain a small fraction of CeO_2 (Fig. 1, S.I. Table 1), though the relative concentrations of this phase were low enough (less than 2 wt% in all compositions) as to make the contributions to the spectra insignificant when considered in the context of the detection limit of Ce L_3-edge XANES. As determined by previous reports of the Ce oxidation state in Ce-brannerite, a small fraction of Ce^{3+} was present in the material batched targeting $CeTi_2O_6$ [16–18, 26], which had an average Ce oxidation state of 3.9(1)+, within the expected range for this material (from 3.85+ to 4.0+ depending on thermal history). The two other compositions forming near-single-phase brannerite, $CeTi_{1.8}Nb_{0.2}O_6$ and $CeTi_{1.6}Nb_{0.4}O_6$, contained Ce in lower overall oxidation states of 3.7(1)+ and 3.5(1)+, respectively, in keeping with their higher Nb contents. The materials targeting $CeTi_{1.4}Nb_{0.6}O_6$ and $CeTi_{1.2}Nb_{0.8}O_6$, containing both brannerite (91.0(3) wt% and 34.4(6) wt%, respectively) and aeschynite (7.2(2) wt% and 65.6(6) wt%, respectively), had overall Ce oxidation states of 3.3(1)+ and 3.1(1)+, respectively. As expected from previous literature, the mean Ce oxidation state in the aeschynite end-member $CeTiNbO_6$ was 3.0(1)+ [27].

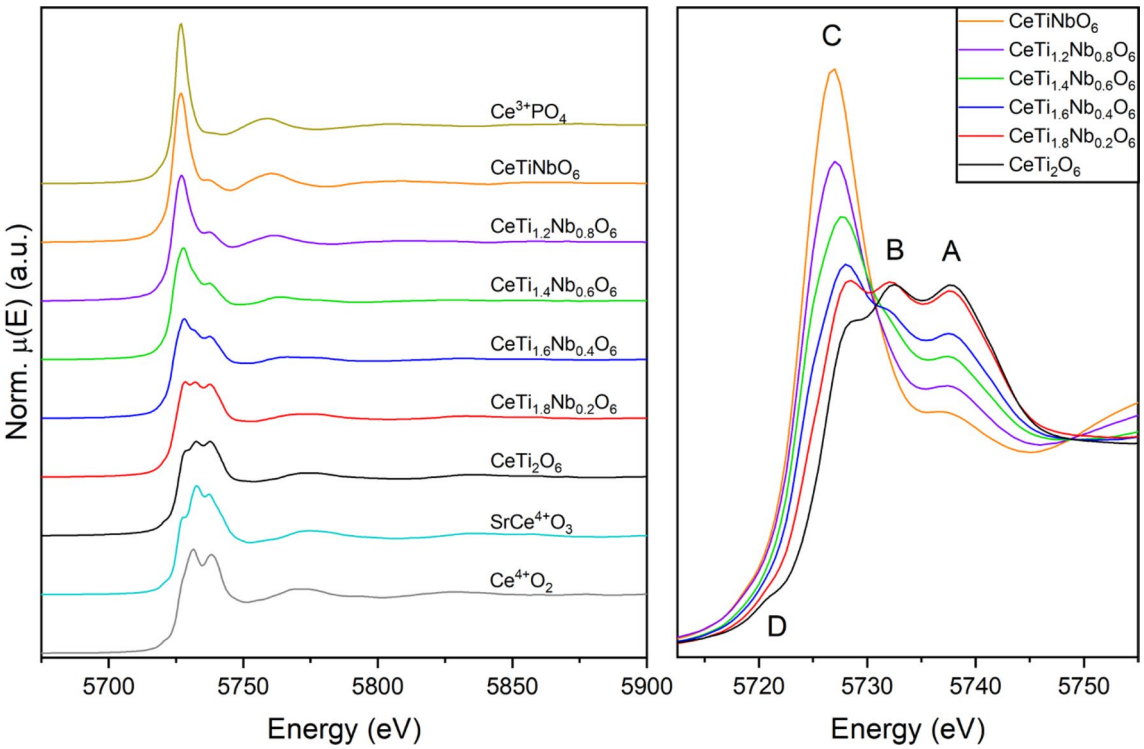

Fig. 4 Left: Ce L_3-edge XANES spectra of materials in the $CeTi_{2-x}Nb_xO_6$ system, alongside $Ce^{4+}O_2$, $SrCe^{4+}O_3$ and $Ce^{3+}PO_4$ reference compounds. Right: detailed view of the edge for the materials produced in this work, with various features marked as discussed in the text

Discussion

Given the previous report of the limited solubility of Nb^{5+} on the Ti-site of the brannerite structure when Al^{3+} was available to ensure charge neutrality, significant solid solubility was not expected at the brannerite-rich end of the $CeTi_{2-x}Nb_xO_6$ compositional series. However, as observed in the phase assemblages here, it appears that, when charge balanced by reduction of Ce^{4+} to Ce^{3+}, the solid solubility of Nb^{5+} is slightly below 0.6 f.u., with the material targeting $CeTi_{1.4}Nb_{0.6}O_6$ comprising brannerite and a small but significant fraction of aeschynite (91.0(3) wt% and 7.2(2) wt%, respectively).

As described above, the mean Ce oxidation state in these materials is dependent on the fraction of Nb^{5+} substituted for Ti^{4+}. In literature reports, the Ce-brannerite end-member usually contains a small fraction of Ce^{3+} as a result of the materials thermal history [16–18, 27], with the material produced in the present study having an average Ce oxidation state of 3.9(1)+. On addition of 0.2 f.u. of Nb^{5+}, the produced material, comprising 99.7(1) wt% brannerite and 0.3(1) wt% CeO_2, had an overall Ce oxidation state of 3.7(1)+. This trend continued as the target Nb incorporation increased, with the average Ce oxidation state decreasing in-line with the nominal Nb content of the material.

Past the limit of solubility of Nb^{5+} in the brannerite structure (*i.e.* in the samples targeting $x = 0.6$, 0.8), an aeschynite structured product was also present. If the assumption is made that all Ce in the aeschynite phases in the materials targeting $CeTi_{1.4}Nb_{0.6}O_6$ and $CeTi_{1.2}Nb_{0.8}O_6$ was present as Ce^{3+} only, approximate calculations give the brannerite phase Ce oxidation state in both materials as approximately 3.4+. This is in good agreement with the observations made above from the phase assemblages and trends in unit cell parameters observed, where it appeared the limit of solid solubility falls at slightly less than 0.6 f.u. of Nb (corresponding to $Ce^{3.4+}$). This assumption does require validation with compositional information for both the brannerite and aeschynite phases produced, as solid solubility of excess Ti would result in an aeschynite Ce oxidation state of greater than 3+.

Conclusions

Though a single phase Ce^{3+} brannerite was not formed, the materials studied here do expand the known crystal chemistry of the brannerite structure significantly. It establishes that, analogous to previously reported $U^{5+}(Ti,Al)_2O_6$ brannerites, average A-site oxidation states of less than 4+ can be stabilised in the brannerite structure when suitable charge-balancing species are available for substitution on the Ti-site. It also establishes that expansion of the A-site past the size of Th^{4+} (the largest previously reported A-site cation(s) in titanate brannerites) is possible [13], with $Ce^{3.4+}$, likely at or close to the limit of stability of Nb-doped Ce-brannerite, having an average ionic radius slightly larger than that of Th^{4+} (0.954 Å compared to 0.94 Å). The Ce-aeschynite structure appears unable to support a significant inventory of Ce^{4+} when charge balanced by excess Ti^{4+} on the Ti/Nb site, within the detection limit of Ce L_3-edge XANES. In contrast, the brannerite structure has been shown here to support a significant inventory of Ce^{3+} when charge balanced by Nb^{5+} on the Ti-site, with the limit of solid solubility just below the target composition $Ce^{3.4+}Ti_{1.4}Nb_{0.6}O_6$.

Given these observations, the use of brannerite-structured materials for immobilisation of Pu and minor actinide wastes comprising mixed 3+ and 4+ cations is possible, though further work examining this and similar systems is necessary prior to full validation with actual Pu or minor actinides.

Supplementary Information The online version contains supplementary material available at https://doi.org/10.1557/s43580-023-00532-2.

Acknowledgments The authors would like to thank Dr. Bruce Ravel for his assistance in collecting the XANES spectra reported here. This work utilised the HADES/MIDAS facility at the University of Sheffield, established with financial support from EPSRC and BEIS, under grant EP/T011424/1 [28]. CLC is grateful to EPSRC for funding under EP/N017374/1. This research used beamline 6-BM of the National Synchrotron Light Source II, a U.S. Department of Energy (DOE) Office of Science User Facility operated for the DOE Office of Science by Brookhaven National Laboratory under Contract No. DESC0012704.

Data availability All data generated or analysed during this study are available from the corresponding author on reasonable request.

Declarations

Conflict of interest On behalf of all authors, the corresponding author states there is no conflict of interest.

References

1. L.R. Blackburn, D.J. Bailey, S.-K. Sun, L.J. Gardner, M.C. Stennett, C.L. Corkhill, N.C. Hyatt, Review of zirconolite crystal chemistry and aqueous durability. Adv. Appl. Ceram. **120**(2), 69–83 (2021). https://doi.org/10.1080/17436753.2021.1877596
2. E.R. Vance, C.J. Ball, R.A. Day, K.L. Smith, M.G. Blackford, B.D. Begg, P.J. Angel, Actinide and rare earth incorporation into zirconolite. J. Alloys Compd. **213–214**, 406–409 (1994). https://doi.org/10.1016/0925-8388(94)90945-8
3. F.W. Clinard, L.W. Hobbs, C.C. Land, D.E. Peterson, D.L. Rohr, R.B. Roof, Alpha decay self-irradiation damage in 238Pu-substituted zirconolite. J. Nucl. Mater. **105**(2), 248–256 (1982). https://doi.org/10.1016/0022-3115(82)90381-6
4. B. Burakov, E. Anderson, M. Yagovkina, M. Zamdryanskaya, E. Nikolaeva, Behavior of 238 Pu-doped ceramics based on cubic zirconia and pyrochlore under radiation damage. J. Nucl. Sci. Technol. **39**(sup3), 733–736 (2002). https://doi.org/10.1080/00223131.2002.10875571
5. R.C. Ewing, W.J. Weber, J. Lian, Nuclear waste disposal—pyrochlore (A2B2O7): nuclear waste form for the immobilization of plutonium and "Minor" actinides. J. Appl. Phys. **95**(11), 5949–5971 (2004). https://doi.org/10.1063/1.1707213
6. Y. Zhang, K.P. Hart, B.D. Begg, E.A. Keegan, A.R. Day, A. Brownscombe, M.W.A. Stewart, Durability of Pu-doped titanate and zirconate ceramics designed for Pu immobilisation. MRS Online Proc. Libr. (2002). https://doi.org/10.1557/PROC-713-JJ6.1
7. D.J. Bailey, M.C. Stennett, B. Ravel, D. Grolimund, N.C. Hyatt, Synthesis and characterisation of brannerite compositions (U0.9Ce0.1)1−xMxTi2O6 (M = Gd3+, Ca2+) for the immobilisation of MOX residues. RSC Adv. **8**(4), 2092–2099 (2018). https://doi.org/10.1039/C7RA11742F
8. S.V. Yudintsev, S.V. Stefanovsky, M.S. Nikolskii, O.I. Stefanovskaya, B.S. Nikonov, Brannerite, UTi2O6: crystal chemistry, synthesis, properties, and use for actinide waste immobilization. Radiochemistry **58**(4), 333–348 (2016). https://doi.org/10.1134/S1066362216040019
9. E.R. Vance, J.N. Watson, M.L. Carter, R.A. Day, B.D. Begg, Crystal chemistry and stabilization in air of brannerite, UTi2O6. J. Am. Ceram. Soc. **84**(1), 141–144 (2001). https://doi.org/10.1111/j.1151-2916.2001.tb00621.x
10. J.W. Wald, P. Offemann, A study of radiation effects in curium-doped Gd2Ti2O7 (Pyrochlore) and CaZrTi2O7 (Zirconolite). MRS Online Proc. Libr. Arch. (1981). https://doi.org/10.1557/PROC-11-369
11. W.J. Weber, J.W. Wald, H.J. Matzke, Effects of self-radiation damage in Cm-doped Gd2Ti207 and CaZrTi207. J. Nucl. Mater. **138**(2), 196–209 (1986). https://doi.org/10.1016/0022-3115(86)90006-1
12. B.D. Begg, E.R. Vance, R.A. Day, M. Hambley, S.D. Conradson, Plutonium and neptunium incorporation in zirconolite. MRS Online Proc. Libr. OPL (1996). https://doi.org/10.1557/PROC-465-325
13. E.R. Vance, M.L. Carter, M.W.A. Stewart, R.A. Day, B.D. Begg, C.J. Ball, Ionic size limits for A ions in Brannerite (ATi2O6) and pyrochlore (CaATi2O7) titanate structures A = tetravalent rare earths and actinides. MRS Online Proc. Libr. OPL (2002). https://doi.org/10.1557/PROC-713-JJ2.6
14. G.J. Thorogood, M. Avdeev, B.J. Kennedy, Structural studies of the Aeschynite-Euxenite transformation in the series Ln(TiTa)O6 Ln=Lanthanide. Solid State Sci. **12**(7), 1263–1269 (2010). https://doi.org/10.1016/j.solidstatesciences.2010.02.036
15. W.L. Gong, R.C. Ewing, L.M. Wang, H.S. Xie, Aeschynite and Euxenite structure-types as host phases for rare-earths and actinides from HLW. MRS Online Proc. Libr. OPL **412**, 377 (1995). https://doi.org/10.1557/PROC-412-377
16. L.T. Huynh, S.B. Eger, J.D.S. Walker, J.R. Hayes, M.W. Gaultois, A.P. Grosvenor, How temperature influences the stoichiometry of CeTi2O6. Solid State Sci. **14**(6), 761–767 (2012). https://doi.org/10.1016/j.solidstatesciences.2012.03.030
17. M.C. Dixon Wilkins, E.R. Maddrell, M.C. Stennett, N.C. Hyatt, The effect of temperature on the stability and cerium oxidation state of CeTi2O6 in inert and oxidizing atmospheres. Inorg. Chem. **59**(23), 17364–17373 (2020). https://doi.org/10.1021/acs.inorgchem.0c02681
18. E.R. Aluri, A.P. Grosvenor, S.H. Forbes, J.E. Greedan, L.M. Bachiu, Assessing the oxidation states and structural stability of the Ce analogue of brannerite. Surf. Interface Anal. **49**(13), 1335–1344 (2017). https://doi.org/10.1002/sia.6265
19. M.C. Dixon Wilkins, L.M. Mottram, E.R. Maddrell, M.C. Stennett, C.L. Corkhill, K.O. Kvashnina, N.C. Hyatt, Synthesis, characterization, and crystal structure of dominant uranium(V) brannerites in the UTi2–XAlxO6 system. Inorg. Chem. **60**(23), 18112–18121 (2021). https://doi.org/10.1021/acs.inorgchem.1c02733
20. Y. Zhang, T. Wei, Z. Zhang, L. Kong, P. Dayal, D.J. Gregg, Uranium Brannerite with Tb(III)/Dy(III) ions: phase formation, structures, and crystallizations in glass. J. Am. Ceram. Soc. **102**(12), 7699–7709 (2019). https://doi.org/10.1111/jace.16657
21. B. Ravel, M. Newville, ATHENA, ARTEMIS, HEPHAESTUS: data analysis for x-ray absorption spectroscopy using IFEFFIT. J. Synchrotron Radiat. **12**(4), 537–541 (2005). https://doi.org/10.1107/S0909049505012719
22. M. Newville, Larch: an analysis package for XAFS and related spectroscopies. J. Phys. Conf. Ser. **430**(1), 012007 (2013). https://doi.org/10.1088/1742-6596/430/1/012007
23. R.D. Shannon, Revised effective ionic radii and systematic studies of interatomic distances in halides and chalcogenides. Acta Crystallogr. A **32**(5), 751–767 (1976). https://doi.org/10.1107/S0567739476001551
24. N. Jiang, D. Su, J.C.H. Spence, Determination of Ti coordination from pre-edge peaks in Ti K-Edge XANES. Phys. Rev. B **76**(21), 214117 (2007). https://doi.org/10.1103/PhysRevB.76.214117
25. F. Farges, G.E. Brown, J.J. Rehr, Ti K-Edge XANES studies of Ti coordination and disorder in oxide compounds: comparison between theory and experiment. Phys. Rev. B **56**(4), 1809–1819 (1997). https://doi.org/10.1103/PhysRevB.56.1809
26. E. Paknahad, A.P. Grosvenor, Investigation of CeTi2O6- and CaZrTi2O7-containing glass-ceramic composite materials. Can. J. Chem. **95**(11), 1110–1121 (2017). https://doi.org/10.1139/cjc-2016-0633
27. R.S. Roth, T. Negas, H.S. Parker, D.B. Minor, C. Jones, Crystal chemistry of cerium titanates, tantalates and niobates. Mater. Res. Bull. **12**(12), 1173–1182 (1977). https://doi.org/10.1016/0025-5408(77)90171-4
28. N.C. Hyatt, C.L. Corkhill, M.C. Stennett, R.J. Hand, L.J. Gardner, C.L. Thorpe, The HADES facility for high activity decommissioning engineering & science: Part of the UK national nuclear user facility. IOP Conf. Ser. Mater. Sci. Eng. **818**, 012022 (2020). https://doi.org/10.1088/1757-899X/818/1/012022